RESEARCH ARTICLE

# Astroglial N-myc downstream-regulated gene 2 protects the brain from cerebral edema induced by stroke

Hang Guo[1,2]    |    Anqi Yin[3,2]    |    Yulong Ma[4]    |    Ze Fan[2]    |    Liang Tao[2]    |
Wenhong Tang[5]    |    Yaqun Ma[1]    |    Wugang Hou[2]    |    Guohong Cai[6]    |    Lixia Zhuo[7]    |
Jian Zhang[8]    |    Yan Li[7,2]    |    Lize Xiong[9,2]

[1]Department of Anesthesiology, The Seventh Medical Center of Chinese PLA General Hospital, Beijing, China

[2]Department of Anesthesiology and Perioperative Medicine, Xijing Hospital, The Air Force Military Medical University, Xi'an, China

[3]Department of Anesthesiology, Jinling Hospital, Nanjing, China

[4]Anesthesia and Operation Center, The First Medical Center of Chinese PLA General Hospital, Beijing, China

[5]Department of Anesthesiology, The 960th Hospital of PLA, Jinan, China

[6]Institute of Neuroscience, The Air Force Military Medical University, Xi'an, China

[7]Department of Anesthesiology & Center for Brain Science, The First Affiliated Hospital of Xi'an Jiaotong University, Xi'an, China

[8]Department of Biochemistry and Molecular Biology, The Air Force Military Medical University, Xi'an, China

[9]Department of Anesthesiology & Translational Research Institute of Brain and Brain-Like Intelligence, Shanghai Fourth People's Hospital, Tongji University School of Medicine, Shanghai, China

**Correspondence**
Yan Li, No. 277, Yanta West Road, Xi'an, Shaanxi 710061, China.
Email: liyanxjtu@xjtu.edu.cn

Lize Xiong, No. 127, Changle West Road, Xi'an, Shaanxi 710032, China.
Email: mzkxlz@126.com, xionglize@tongji.edu.cn;

## Abstract

Brain edema is a grave complication of brain ischemia and is the main cause of herniation and death. Although astrocytic swelling is the main contributor to cytotoxic edema, the molecular mechanism involved in this process remains elusive. *N-myc downstream-regulated gene 2* (*NDRG2*), a well-studied tumor suppressor gene, is mainly expressed in astrocytes in mammalian brains. Here, we found that NDRG2 deficiency leads to worsened cerebral edema, imbalanced $Na^+$ transfer, and astrocyte swelling after ischemia. We also found that NDRG2 deletion in astrocytes dramatically changed the expression and distribution of aquaporin-4 and $Na^+$-$K^+$-ATPase $\beta1$, which are strongly associated with cell polarity, in the ischemic brain. Brain edema and astrocyte swelling were significantly alleviated by rescuing the expression of astrocytic $Na^+$-$K^+$-ATPase $\beta1$ in NDRG2-knockout mouse brains. In addition, the upregulation of astrocytic NDRG2 by lentiviral constructs notably attenuated brain edema, astrocytic swelling, and blood–brain barrier destruction. Our results indicate a particular role of NDRG2 in maintaining astrocytic polarization to facilitate $Na^+$ and water transfer balance and to protect the brain from ischemic edema. These findings provide insight into NDRG2 as a therapeutic target in cerebral edema.

# 1 | INTRODUCTION

Brain edema, a serious consequence of cerebral stroke, trauma, infection, and tumor, is implicated in elevated intracranial pressure and may lead to brain herniation and death (Wijdicks et al., 2014). In the past few decades, the treatment of cerebral edema has been limited to osmotherapy and surgical decompression (Cordonnier, Demchuk, Ziai, & Anderson, 2018; Esquenazi, Lo, & Lee, 2017; Winkler, Minter, Yue, & Manley, 2016). However, these treatments are based on symptoms and can lead to water-electrolyte imbalance and even craniotomy (Dharmasaroja, 2016).

As the largest cell population in the central nervous system (CNS), astrocytes perform many housekeeping functions, including formation of the blood–brain barrier (BBB), regulation of neuronal metabolism and cerebral blood flow, and maintenance of water balance, ion homeostasis, and osmotic pressure (Ransom & Ransom, 2012; Thrane, Rangroo Thrane, & Nedergaard, 2014). Accumulating evidence shows that changes in astrocytic structure and functional polarization are implicated in the dynamic process of brain edema (Steiner et al., 2012; Wang & Parpura, 2016). Every astrocyte has at least one process that encases a microvessel and is called an astrocytic end-foot; the end-feet are enriched in water and ion channels, such as aquaporin-4 (AQP4), $Na^+$, $K^+$, and $Cl^-$ ion channels and transporters, to maintain the water and ion balance. Astrocytic processes expand or retract from neurons and blood vessels and dramatically regulate neural activity and the integrity of the BBB (Nico & Ribatti, 2012). Furthermore, astrocytes also play an important role in cerebral edema upon various brain injury challenges (Hertz et al., 2014). Known as cytotoxic swelling, astrocytes swell rapidly in the early stage of edema after acute pathological states, such as ischemia and traumatic brain injury (Gorse, Lantzy, Lee, & Lafrenaye, 2018; Jayakumar et al., 2014; Kimelberg, 2005).

N-myc downstream-regulated gene 2 (NDRG2), known as a tumor suppressor gene (Hwang et al., 2011; Yao, Zhang, & Liu, 2008), was first identified in 2003 to be highly expressed in the human brain (Deng et al., 2003). NDRG2 is primarily and specifically expressed in astrocytes in various brain areas (Ma et al., 2014; Nichols, 2003; Takeichi et al., 2011). Furthermore, NDRG2 was found to regulate astrocytic activation and stabilize astrocytic morphology (Takeichi et al., 2011). NDRG2 has even been identified as a unique marker for astrocytes (Flügge, Araya-Callis, Garea-Rodriguez, Stadelmann-Nessler, & Fuchs, 2014). In transient focal cerebral ischemia, the expression of NDRG2 increases, and NDRG2 translocates from the cytoplasm to the nucleus (Li et al., 2011). Recently, NDRG2 was reported to be involved in maintaining the structure of the BBB after ischemia by down-regulating matrix metalloproteinases (Takarada-Iemata et al., 2018). BBB breakdown and leakage following stroke can cause brain edema. However, the role of NDRG2 in ischemic brain edema remains unclear.

Here, we provide evidence to support the critical role of astroglial NDRG2 in sustaining astrocytic polarization and regulating astrocyte-associated water-sodium balance under physiological and pathological conditions. NDRG2 is an endogenous neuroprotector and a promising target for the intervention of ischemic brain edema.

# 2 | MATERIALS AND METHODS

## 2.1 | Animals

Animals were housed under a regular 12-hr light/dark cycle with access to food and water ad libitum. $Ndrg2^{flox/flox}$ mice were crossed to B6.C-Tg(CMV-cre)1Cgn/J mice (Jackson Labs) to generate $Ndrg2^{-/-}$ mice. The line was backcrossed to C57BL/6J more than 20 times. pAAV-CAG-Cre-3flag virus was injected into the right lateral cerebral ventricle of $Ndrg2^{flox/flox}$ mice to conditionally knock out the expression of NDRG2 in astrocytes (referred to as $Ndrg2^{GFAP}$ cKO). Young adult male (8 to 10 weeks old) mice were used in this study. We made all efforts to minimize the number of mice used and their suffering. The experimental protocols were reviewed and approved by the Ethics Committee of the Fourth Military Medical University.

## 2.2 | Transient focal cerebral ischemia and reperfusion

Transient focal cerebral ischemia was induced by middle cerebral artery occlusion and reperfusion (tMCAO). Mice were anesthetized with 1.5% isoflurane. Body temperature was continuously monitored and maintained between 36.5 and 37.5°C with a thermostatic blanket. Surgery was performed under a Zeiss surgical microscope. Cerebral cortical perfusion was monitored by laser-Doppler flowmetry. Mice were placed in the supine position, and the right carotid bifurcation was exposed. Then, the right external carotid artery (ECA) and the right internal carotid artery were exposed and carefully freed from the adjacent vagus nerve. After occlusion of the common carotid artery with a microclip, the right ECA was ligated. A small incision was made in the ECA, and an 8-0 nylon thread with a silicone-coated tip was inserted into the ECA and gently advanced through the internal carotid artery until its tip occluded the origin of the middle cerebral artery (MCA). Correct placement of the suture was indicated by a sudden drop in the local cortical blood flow in the right MCA territory to approximately 15–20% of baseline as monitored by laser-Doppler flowmetry. After successful occlusion, the monofilament was secured in place by ligation, and the incision was closed with microsurgical clips. After 60 min of occlusion, each mouse was

reanesthetized to facilitate the removal of the occlusion and underwent reperfusion for 24 hr.

## 2.3 | Brain water content

Mice were anesthetized, and their brains were rapidly dissected. An investigator blinded to the experimental grouping weighed the isolated cerebral cortices to obtain the wet mass and then processed the brains concurrently in a vacuum oven (Savant Speed Vac SC110) for 12 hr at −1,000 mbar (Savant VP Two Stage Vacuum Pump) to completely desiccate the cortices and obtain the dry mass. The percentage of brain water content was calculated as follows: (wet mass − dry mass) × 100/(wet mass).

## 2.4 | Transmission electron microscopy and immunoelectron microscopy

Mice were anesthetized and intracardially perfused with 0.1 M phosphate-buffered solution (PBS) containing 4% paraformaldehyde (PFA) and 2.5% glutaraldehyde. The penumbra of mice in the tMCAO groups or corresponding tissues from mice in the sham groups were dissected and postfixed overnight at 4°C. Tissues were cut along the coronal plane at a thickness of 50 μm. Samples were processed as previously described (Relucio, Menezes, Miyagoe-Suzuki, Takeda, & Colognato, 2012). For immunoelectron microscopy (IEM), brain tissues were fixed in 4% warm PFA for 6 hr. Subsequently, the tissues were sectioned and stained for AQP4 (1:200; Abcam) or Na$^+$-K$^+$-ATPase $\beta$1 (1:50; Sigma-Aldrich) followed by incubation with Nanogold-conjugated secondary antibody (1:100 Nanoprobes). Gold particles were enhanced with an HQ Silver Enhancement Kit (Nanoprobes). Processed samples were examined and photographed using a JEM-1230 transmission electron microscopy (TEM). The astrocytic foot-process cross-sectional area-lumen perimeter ratio was estimated using the ImageJ Processing and Analysis Program. All data were analyzed and quantified by an investigator blinded to the experimental grouping.

## 2.5 | BBB permeability assays

BBB permeability was quantified by the permeability of tracers. A 45 mg/kg dose of 30 g/L Evans blue dye (Sigma-Aldrich) or 200 μL of 1 mg/ml dextran-tetramethylrhodamine (Invitrogen) injected via the tail vein was circulated for 2 hr before animals underwent sham or tMCAO operations. Then, mice were deeply anesthetized, perfused and fixed with 4% PFA. For fluorescence measurements, brains were frozen and embedded in TissueTek OCT. Frozen tissues were coronally sectioned to a thickness of 12 μm and sealed in a light-tight container.

Evans blue dye was visualized using a fluorescence microscope (BX-51; Olympus, Tokyo, Japan). The red-stained area was defined as BBB permeable. The BBB-permeable area in the right hemisphere and total area in the left hemisphere were measured using Adobe

Photoshop CS5 by an investigator blinded to the experimental grouping. The BBB-permeable area of the right hemisphere and total volume of the left hemisphere were calculated as follows: $V_R = R \times$ slice thickness (12 μm) and $V_L = L \times$ slice thickness (12 μm). The Evans blue-positive area was measured as follows: % $V_P = 100 \times (V_L - V_R)/V_L$.

Dextran-tetramethylrhodamine-injected mouse brain coronal slices were subjected to immunofluorescence for CD31 to visualize the blood vessels. Images were acquired by an investigator blinded to the experimental grouping using a laser scanning confocal microscope (Olympus FV-1000MPE).

## 2.6 | Morphometric analysis of vasculature

Mouse brain coronal sections (20 μm) were stained for the vasculature marker CD31. The capillary density and diameter were imaged (Nikon Fluo View FV1000 laser scanning confocal microscope) and quantified (maximal projection images). Capillary density was quantified using MetaMorph software (Universal Imaging, Downingtown, Pennsylvania) by measuring the area occupied by CD31-positive vessels per field. The mean capillary diameter was measured from cross-sectional vascular profiles by the ImageJ Processing and Analysis Program. Quantification was carried out blindly.

## 2.7 | Primary astrocyte culture

Meninges-free mouse brain cortical tissue was dissected, mechanically dissociated and trypsinized (0.25% in phosphate-buffered saline) to generate a cell suspension. The cells were cultured in poly-L-lysine high-glucose Dulbecco's modified Eagle's medium (Gibco) containing 10% fetal calf serum at 37°C in 5% CO$_2$ and 90% relative humidity. The medium was changed every 3–4 days for 10–14 days to obtain mixed glial cultures. Then, flasks were placed onto a thermostatic shaker at 37°C and 200 rpm/min for 16–18 hr to remove the oligodendrocyte progenitor cells and microglia. More than 95% of the cultures were astrocytes, as determined by immunofluorescent staining with glial fibrillary acidic protein (GFAP) and NDRG2 (Figure S1). Then, the cells were seeded onto laser confocal-specific dishes for immunofluorescence assays.

## 2.8 | Immunofluorescence

Immunofluorescence studies were performed on frozen coronal sections of mouse brains or on primary cultured astrocytes plated on laser confocal-specific dishes. Mice were subjected to cardiac perfusion with 0.1 M PBS followed by fixation with 4% PFA. Brains were removed, and tissues were frozen and embedded in TissueTek OCT. Frozen tissues were cryosectioned at a thickness of 12 μm. The primary cultured astrocytes were plated at a density of $1 \times 10^4$ cells/dish. The cells were fixed with 4% PFA at room temperature for 15 min. Sections/cells were washed with 0.1 M PBS and incubated at 4°C for 12 hr with the following primary antibodies (Table S1): rabbit anti-NDRG2, mouse

anti-NDRG2, mouse anti-GFAP, rat anti-CD31, rabbit anti-AQP4, or mouse anti-Na$^+$-K$^+$-ATPase $\beta$1. Sections/cells were then washed with 0.1 M PBS, followed by incubation at room temperature for 2 hr with the appropriate secondary antibodies as follows: anti-mouse fluorescein isothiocyanate (FITC)-tagged, anti-mouse CY3-tagged, anti-rabbit CY3-tagged, or anti-rat FITC-tagged. Sections/cells were then washed with 0.1 M PBS, and the nuclei were counterstained with 10 μg/ml 4′,6-diamidino-2-phenylindole (DAPI) in 0.1 M PBS for 2 hr at room temperature. The sections/cells were mounted with 50% glycerol and photographed under a laser scanning confocal microscope.

## 2.9 | The length and number of astrocyte processes

Image processing was performed using ImageJ software (Schindelin et al., 2012) by an investigator blinded to the experimental grouping. Primary cultured astrocytes were subjected to immunofluorescence for GFAP to visualize the cytoskeleton with DAPI-stained nuclei. Astrocytes were selected when they fulfilled the following criteria: (a) GFAP staining along the entire arborization field and (b) relative isolation from neighboring astrocytes to avoid overlap. The GFAP signal was segmented with the threshold tool and converted to a binary mask with a skeletonize tool, which allowed us to obtain the segment length and bifurcation of the skeletonized image for analysis with ImageJ software. Then, the lengths and numbers of branches of astroglial processes were measured with ImageJ. The length of the branches was defined as the distance of major processes, which were considered as the dendrites originate from the cell body (proximal) to the tip of the main apical shaft (Pillai et al., 2012). The number and length of the major processes were visualized and qualified using ImageJ by an investigator blinded to the experimental grouping.

## 2.10 | AQP4 clusters along astrocytic end-feet

AQP4 clusters on primary astrocytes were detected on images following intensity thresholding using the ImageJ Processing and Analysis Program. Cluster areas were defined as areas of intense AQP4 immunoreactivity as determined by uniformly applied intensity thresholding. The area occupied by these intensely AQP4 immunoreactive regions was calculated per astrocyte.

## 2.11 | Immunoblotting analysis

The expression of NDRG2, AQP4, Na$^+$-K$^+$-ATPase $\alpha$1, and Na$^+$-K$^+$-ATPase $\beta$1 was detected in mouse brain tissues or primary astrocytes homogenized in RIPA lysis buffer (Beyotime, China) with ×1 Roche complete protease inhibitor cocktail (Roche Diagnostics) and 1 mM phenylmethylsulfonyl fluoride (Beyotime, China). Immunoblotting was performed using the following primary antibodies (Table S1): mouse anti-NDRG2, rabbit anti-NDRG2, mouse anti-Na$^+$-K$^+$-ATPase $\alpha$1,

mouse anti-Na$^+$-K$^+$-ATPase $\beta$1, or rabbit anti-AQP4. Secondary horseradish peroxidase-conjugated goat anti-rabbit or goat anti-mouse antibody was used. Protein bands were visualized using a LI-COR Odyssey System (LI-COR Biotechnology).

## 2.12 | Intracellular Na$^+$

Astrocytes were washed twice in 0.1 M PBS, and then CoroNa Green indicator (Invitrogen) and sulforhodamine 101 (SR 101, MedChemExpress) were added at 1 μM by dilution of a concentrated stock solution in DMSO. Cells were incubated for 30 min at 37°C. The loaded cells were washed twice with 0.1 M PBS before fluorescence was measured. Subsequently, the CoroNa Green indicator was excited at 492 nm, and emission was recorded above 516 nm. SR 101 was excited at 586 nm, and emission was recorded above 605 nm. The images were observed and captured using a laser scanning confocal microscope.

## 2.13 | Statistical analysis

All experiments were performed a minimum of three times. The data were reported as the mean ± $SD$ or mean ± $SEM$, and the analysis was performed using GraphPad Prism 6.0 software. The significance of the differences was determined using Student's two-tailed $t$ test or one-way analysis of variance (ANOVA). A $p$ value <.05 was considered to indicate statistical significance.

## 3 | RESULTS

### 3.1 | NDRG2 deficiency aggravates brain edema and astrocytic swelling following ischemia

NDRG2, a previously known tumor suppressor, is mainly expressed in astrocytes in mammalian brains, and its expression is increased after ischemia. To investigate the role of NDRG2 in ischemic brain edema, we constructed an adeno-associated virus (AAV), pAAV-CAG-MCS-EGFP-3flag, as a control virus and pAAV-CAG-Cre-3flag to conditionally knock out the expression of astrocytic NDRG2. pAAV-CAG-MCS-EGFP-3flag or pAAV-CAG-Cre-3flag was injected into the right lateral cerebral ventricle of $Ndrg2^{flox/flox}$ mice. Three weeks later, NDRG2, GFAP, and EGFP were detected in different brain regions by immunofluorescence staining and immunoblotting. NDRG2 (red) was colocalized with EGFP (green) in the control groups, indicating that the AAV virus is specifically enriched in NDRG2-labeled astrocytes. NDRG2-positive astrocytes and NDRG2 protein were dramatically reduced in brains from NDRG2 knockout mice (hereafter referred to as $Ndrg2^{GFAP}$ cKO) compared with control mouse brains (Figure S2). $Ndrg2^{GFAP}$ cKO mice and control mice underwent a 60 min middle cerebral artery occlusion (MCAO) surgery followed by 24 hr reperfusion, and the brain water content was then detected (Figure 1a). We found that the percentage of brain water content was significantly

**FIGURE 1** NDRG2 deficiency exacerbates brain edema and astrocyte swelling after stroke. (a) Quantification of brain water content in cortices isolated from *Ndrg2*$^{GFAP}$ *cKO* mice (CreV-N2) and control mice (ConV) in sham groups and MCAO groups. Data are shown as the mean ± *SD* (*n* = 5–6). *$p$ < .05, **$p$ < .01 versus sham mice, ##$p$ < .01 versus control mice. (b) Representative transmission electron micrographs showing the swollen perivascular astrocytic end-feet area (blue area). A: astrocyte end-feet; B: basal lamina; E: endothelial cell; L: lumen. Scale bar = 2 μm. (c) Astrocyte end-feet area-to-capillary lumen perimeter ratio. Data are shown as the mean ± *SD* (*n* = 5–6). *$p$ < .05, **$p$ < .01 versus sham mice, ##$p$ < .01 versus control mice. (d) High-magnification images of ultrastructural changes in MCAO group mice. Red arrowheads indicate disruption of the plasma membrane, basal membrane, gap junctions, organelles, accumulation of glycogen, and swollen endothelial cytoplasm. Scale bar = 0.5 μm [Color figure can be viewed at wileyonlinelibrary.com]
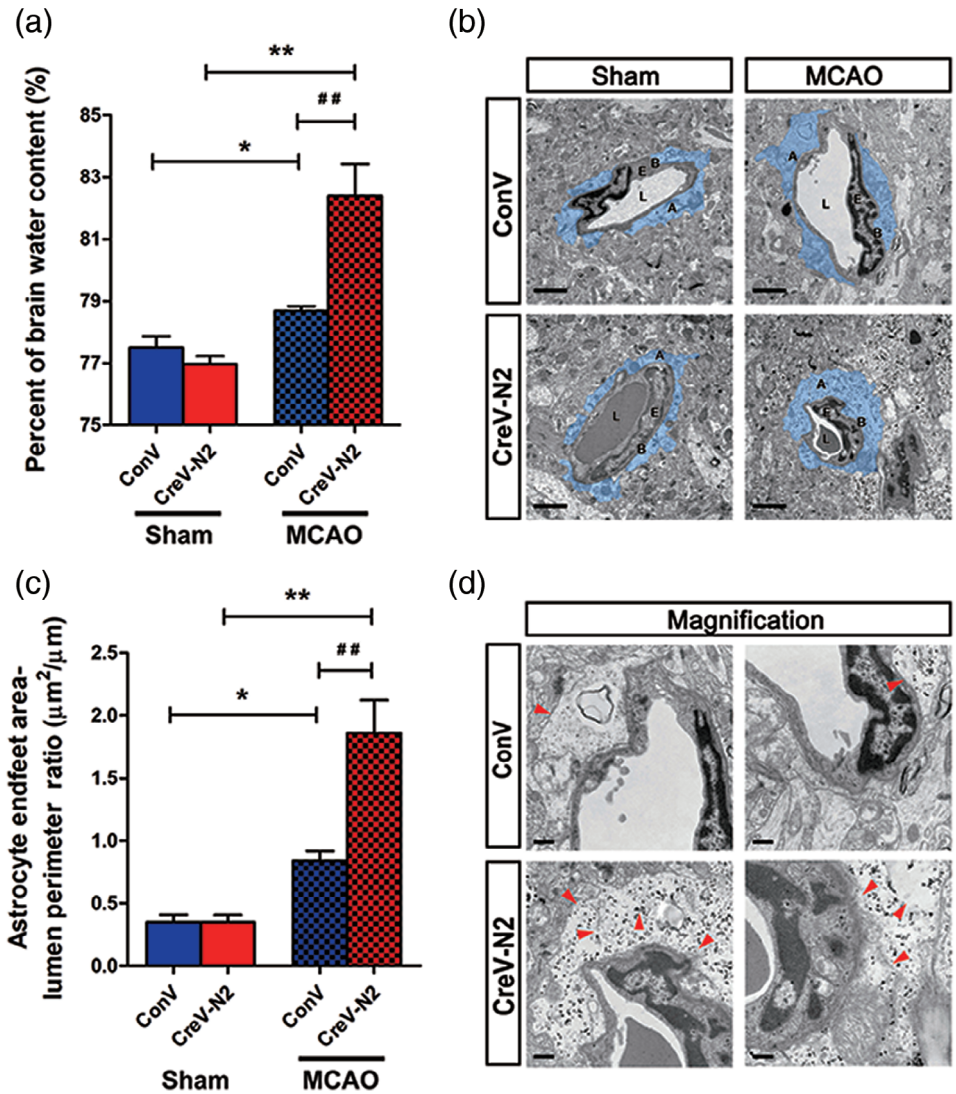


elevated in the transient MCAO groups compared with the sham groups. The percentage of brain water content in the *Ndrg2*$^{GFAP}$ *cKO* mice was significantly increased compared with that in the control mice after brain ischemia.

Disruption of the BBB is the main pathological basis of ischemic brain edema, so we investigated the effects of NDRG2 deficiency on the BBB structure. Using TEM, we detected the BBB ultrastructure in two groups of mice. No obvious difference in the BBB ultrastructure was observed between *Ndrg2*$^{GFAP}$ *cKO* mice and control mice under physiological conditions (Figure S3a,b). However, striking differences emerged after ischemic injury. Swollen astrocyte end-feet were clearly detected in the ischemic penumbra of both groups, especially the astrocyte end-foot area-to-capillary lumen cross length ratio, which was significantly higher in NDRG2 knockout mice than in control mice (Figure 1b,c). Magnified images showed that astrocyte processes exhibited increased swelling, discontinuous plasma membranes, disturbed gap junctions, broken organelles, swollen endothelial cytoplasm and rough basal membranes, which were indicators of a severely compromised BBB in *Ndrg2*$^{GFAP}$ *cKO* mice (Figure 1d). These

data together suggest that NDRG2 deficiency aggravates brain edema, astrocyte end-feet swelling and BBB disorganization after ischemic brain injury.

## 3.2 | NDRG2 deletion exacerbates the destruction of the BBB after stroke

A previous study reported that astrocyte end-feet cover more than 99% of brain capillaries, participating in BBB structural formation and functional performance (Jukkola & Gu, 2015; Mathiisen, Lehre, Danbolt, & Ottersen, 2010). We suspected that severe BBB leakage is accompanied by swollen astrocytic end-feet and leads to an increase in brain water content in *Ndrg2*$^{GFAP}$ *cKO* mice after tMCAO. To address this hypothesis, brain vascular patterning and BBB permeability were examined in *Ndrg2*$^{GFAP}$ *cKO* and control mice after tMCAO. No significant differences in vascular patterns were visualized by immunofluorescence for the vascular marker CD31, including vascular density and vascular diameter, under physiological
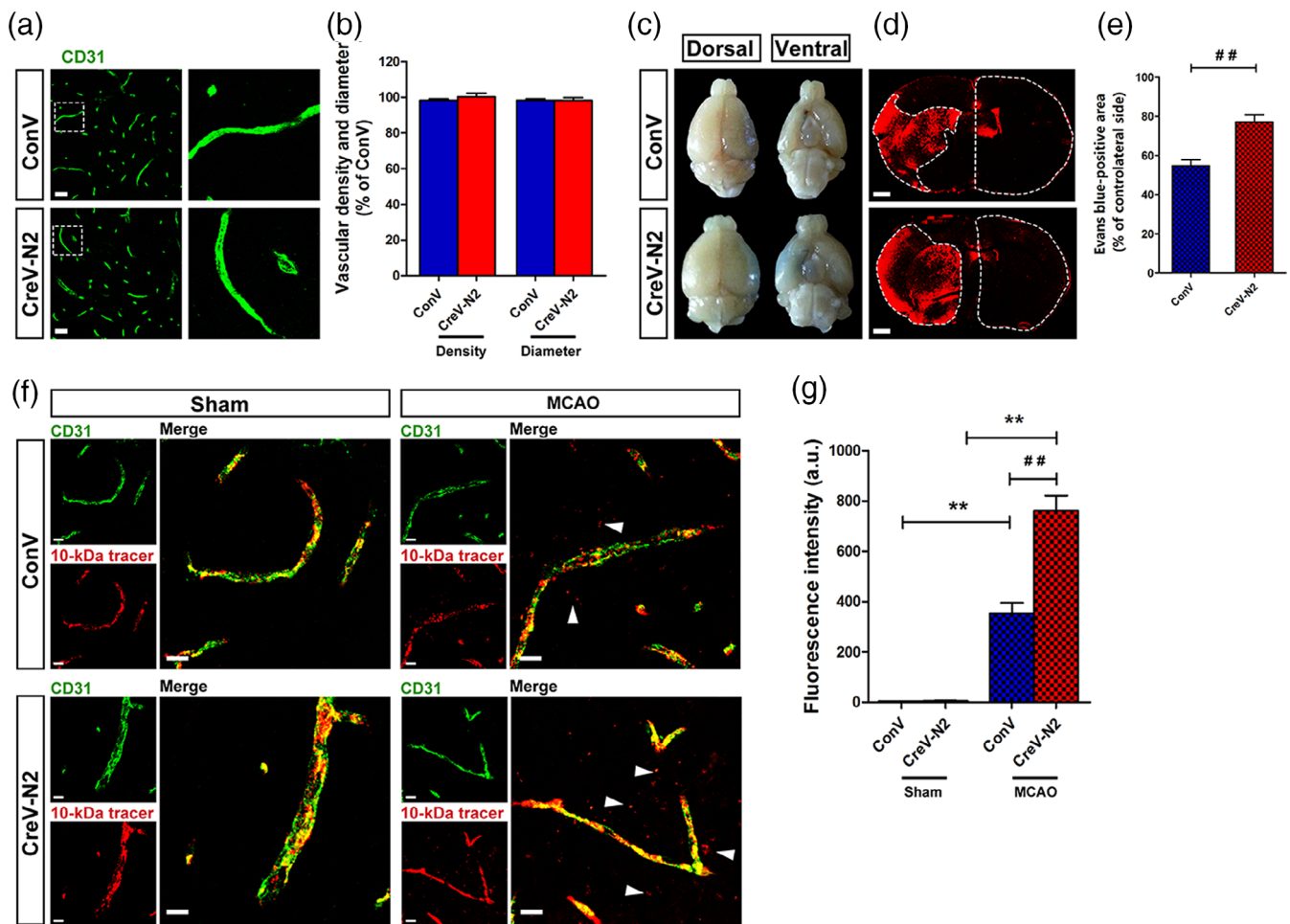
**FIGURE 2** NDRG2 knockout causes a breakdown of the blood–brain barrier after MCAO. (a) Images of cortical vascular staining for CD31. Scale bar = 30 μm. (b) No abnormalities were found in the cortical capillary density and diameter of $Ndrg2^{GFAP}$ cKO mice and control mice under normal conditions. (c) The tracer, Evans blue dye, permeates into the brain parenchyma after MCAO ($n$ = 3). (d) Representative images of coronal sections from mice that underwent MCAO after injection of Evans blue dye; fluorescence-positive areas in $Ndrg2^{GFAP}$cKO mice (bottom) and control mice (top) observed by microscopy. Scale bar = 500 μm. (e) Evans blue-positive area percentage of the contralateral side. Data are shown as the mean ± SD ($n$ = 8). [##]$p$ < .01 versus control mice. (f) The 10-kDa molecular weight tracer was confined to vessels in sham mice, whereas it leaked out of the vessels (white arrowheads) in the penumbra of mice that underwent MCAO. Green, CD31; red, tracer. Scale bar = 10 μm. (g) Quantification of tracer fluorescence density (INT/mm²). **$p$ < .01 versus sham mice, [##]$p$ < .01 versus control mice [Color figure can be viewed at wileyonlinelibrary.com]

conditions (Figure 2a,b). However, a more seriously impaired BBB was present in the ischemic penumbra of $Ndrg2^{GFAP}$ cKO mice compared with that of control mice, as demonstrated by the permeation of Evans blue dye from the bloodstream into the brain parenchyma (Figure 2c–e).

To further observe the local disruption of the astrocyte-endothelial cell interactions along vessels, we examined the leakage of dextran-tetramethylrhodamine (MW, 10 kDa) from blood vessels. No leakage was observed in the cortical areas of the sham groups. However, after tMCAO, the leakage of dextran-tetramethylrhodamine from the vasculature in the ischemic penumbra was significantly increased in $Ndrg2^{GFAP}$ cKO mice compared with control mice (Figure 2f,g). The increased leakage of Evans blue dye and the 10-kDa tracer into the brain parenchyma from the blood vessels in $Ndrg2^{GFAP}$ cKO mice suggests that NDRG2 deficiency causes exacerbated BBB

structural impairment and functional integrity destruction after ischemia reperfusion injury.

## 3.3 | NDRG2 is required for maintaining astrocytic polarity

Maintaining the appropriate morphology and polarity of astrocytes is critical for astrocytic function and homeostasis (Etienne-Manneville, 2008; Nagelhus & Ottersen, 2013; Wolburg, Noell, Wolburg-Buchholz, Mack, & Fallier-Becker, 2009). Recent studies identified that a loss of astrocyte polarization is a common feature in many neurological diseases, including ischemic brain damage, mesial temporal lobe epilepsy and Alzheimer's disease (Alvestad et al., 2013; Eid et al., 2005; Frydenlund et al., 2006; Yang et al., 2011). Therefore, we

investigated the effects of NDRG2 on astrocyte morphology and polarity in highly pure GFAP-positive astrocyte cultures, which were more than 95% GFAP-positive (Figure S1). Primary cultured astrocytes from NDRG2 knockout ($Ndrg2^{-/-}$) mice (Li et al., 2017)

exhibited fewer and shorter processes and lower levels of phalloidin than primary cultured astrocytes from $Ndrg2^{flox/flox}$ mice (Figure 3a–d). The water channel protein AQP4 is an important molecule that reflects the polarization of astrocytes. AQP4 has been identified to
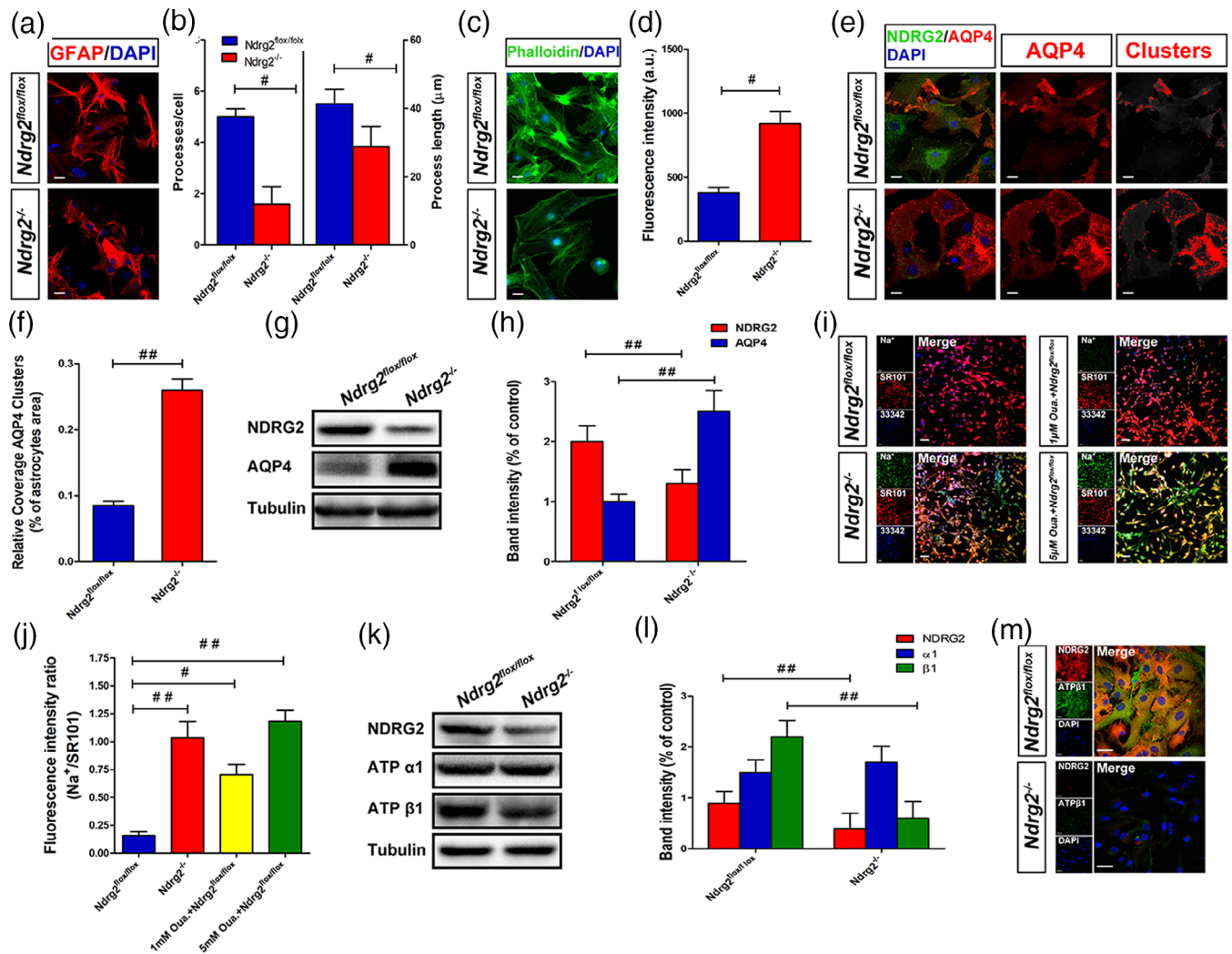


**FIGURE 3** NDRG2 maintains the polarity of astrocytes under physiological conditions. (a) Primary cultured $Ndrg2^{-/-}$ astrocytes and control astrocytes were fixed and subjected to immunostaining for GFAP (red) and DAPI (blue), scale bar = 20 μm. (b) Number/cell and length of the major processes of at least 25 astrocytes. $^{#}p < .05$ versus control astrocytes. (c) Primary cultured $Ndrg2^{-/-}$ astrocytes and control astrocytes were fixed and subjected to immunostaining for phalloidin (green) and DAPI (blue), scale bar = 20 μm. (d) Green fluorescence intensity of phalloidin in each group. Data are presented as the mean ± SEM of three independent experiments, each performed in five fields of view. $^{#}p < .05$ versus control astrocytes. (e) Immunofluorescence was used to detect NDRG2 (green) and AQP4 (red) in $Ndrg2^{-/-}$ astrocytes and control astrocytes, and nuclei were labeled blue by DAPI. AQP4 assembled in clusters was detected in $Ndrg2^{-/-}$ astrocytes. Colorized AQP4 clusters (right, red) depict regions where the AQP4 immunoreactivity intensity was above the threshold value. Scale bar = 20 μm. (f) Quantification of relative coverage by AQP4 clusters in $Ndrg2^{-/-}$ astrocytes and control astrocytes. Data are presented as the mean ± SEM of three independent experiments, each performed in 5 fields of view. $^{##}p < .01$ versus control astrocytes. (g) Representative Western immunoblots for NDRG2, AQP4 and tubulin of $Ndrg2^{-/-}$astrocytes and control astrocytes. (h) Densitometric quantification of NDRG2 and AQP4 protein expression is shown normalized to tubulin. Data are expressed as the mean ± SEM of three independent experiments. $^{##}p < .01$ versus control astrocytes. (i) Representative fluorescence images showing CoroNa Green (sodium indicator) and SR101 ($Na^+$-insensitive fluorescent dye) trapped inside astroglial cytoplasm and counterstained with Hoechst 33342. Scale bar = 50 μm. (j) Fluorescence intensity ratio of CoroNa Green to SR101 in each group shown in (i). Data are presented as the mean ± SEM of three independent experiments, each performed in five fields of view. $^{#}p < .05$, $^{##}p < .01$ versus control astrocytes. (k) Representative Western immunoblots for NDRG2, ATP α1, ATP β1, and tubulin of $Ndrg2^{-/-}$ astrocytes and control astrocytes. (l) Densitometric quantification of NDRG2, ATP α1, and ATP β1 protein expression is shown normalized to tubulin. Data are expressed as the mean ± SEM of three independent experiments. $^{##}p < .01$ versus control astrocytes. (m) Primary cultured astrocytes were immunolabeled for NDRG2 (red) and ATP β1 (green), and nuclei were labeled blue by DAPI. Scale bar = 30 μm [Color figure can be viewed at wileyonlinelibrary.com]

form clusters, termed orthogonal arrays of particles (OAPs), in the plasma membranes of astrocytes to enhance water transport through the membrane and maintain astrocyte polarization (Nagelhus & Ottersen, 2013). AQP4 plays a key role in the regulation of brain water homeostasis, which is its primary role in the brain (Badaut, Fukuda, Jullienne, & Petry, 2014; Haj-Yasein et al., 2011; Kitchen et al., 2020; Nagelhus & Ottersen, 2013). A recent study showed that brain edema is closely related to the incorporation of additional cytoplasmic AQP4 and the redistribution of AQP4 in the existing OAPs in cultured astrocytes (Michael et al., 2014; Lisjak, Potokar, Rituper, Jorgačevski, & Zorec, 2017). We examined the distribution of AQP4 and NDRG2 in cultured primary astrocytes. Uniform intensity thresholding was used to determine the AQP4 cluster areas, and we found intense AQP4 cluster immunosignals in $Ndrg2^{-/-}$ astrocytes (Figure 3e,f). Immunoblotting analysis showed that AQP4 protein expression was significantly increased in $Ndrg2^{-/-}$ astrocytes compared to the control astrocytes (Figure 3g,h). Together, these results indicate that NDRG2 deficiency may alter the polarization and water balance of astrocytes.

Na$^+$/K$^+$ ATPase is present in all higher eukaryotes and participates in the maintenance of membrane resting potential, cell volume regulation and signal transduction (Dlouha et al. Dlouhá, Teisinger, & Vyskocil, 1979; Quinton & Tormey, 1976; Robinson, 1975). Na$^+$/K$^+$ ATPase is considered one of the most important players in intracellular Na$^+$ signaling, with its prominent role in cellular (patho)physiology. The increase in cytoplasmic sodium causes intracellular hyperosmolality, which induces water influx and cytotoxic edema (Rungta et al., 2015). Therefore, Na$^+$ imaging is an essential technique for the visualization of Na$^+$/K$^+$ ATPase function in vitro. Recent research indicates that an increased intracellular Na$^+$ concentration ($[Na^+]_i$) in astrocytes is associated with the development of brain edema under ischemic brain injury (Minieri, Pivonkova, Harantova, Anderova, & Ferroni, 2015). Here, we measured the fluorescence signals of CoroNa Green, a Na$^+$ indicator dye, to reflect Na$^+$/K$^+$ ATPase function in cultured astrocytes. SR 101, a Na$^+$-insensitive fluorescent dye, was used to normalize the CoroNa Green signals. Fluorescence imaging analysis revealed a substantial $[Na^+]_i$ increase in NDRG2-deficient astrocytes (Figure 3i,j). $Ndrg2^{flox/flox}$ astrocytes responded with a progressive accumulation of CoroNa Green fluorescence after Ouabain (a Na$^+$/K$^+$ ATPase-specific inhibitor) treatment, indicating an elevation of $[Na^+]_i$ caused at least partially by the inhibition of Na$^+$/K$^+$ ATPase function. Moreover, the protein levels of Na$^+$/K$^+$ ATPase α1 and β1 were quantified by immunoblotting. Na$^+$-K$^+$-ATPase β1 protein levels were significantly decreased in $Ndrg2^{-/-}$ astrocytes compared with control astrocytes, whereas no striking difference was observed in the protein level of Na$^+$-K$^+$-ATPase α1 (Figure 3k,l). Double-labeling immunofluorescence showed that Na$^+$-K$^+$-ATPase β1 (green) immunoreactivity was reduced in $Ndrg2^{-/-}$ astrocytes compared with control astrocytes (Figure 3m). These data are consistent with our previous report showing that NDRG2 inhibits the degradation and prolongs the half-life of Na$^+$-K$^+$-ATPase β1 in human salivary cells (Li et al., 2011). Together, these data suggest that NDRG2 maintains, at least partially, the polarization and aquaporin functional homeostasis of astrocytes under physiological conditions.

## 3.4 | Na$^+$-K$^+$-ATPase β1 rescues NDRG2 deficiency-mediated BBB disturbance and brain edema following stroke

To investigate whether NDRG2 is required for maintaining the polarity and function of astrocytes under pathological conditions, IEM was used to visualize the subcellular distribution of AQP4 and Na$^+$-K$^+$-ATPase β1 in perivascular astrocytes in the ischemic penumbra. Gold particles indicated the presence of AQP4 and Na$^+$-K$^+$-ATPase β1 (Figure 4a). AQP4 was evenly distributed on the astrocytic membrane facing the basal lamina of the capillaries in the sham groups. AQP4 was enriched in $Ndrg2^{GFAP}$ cKO mice compared with control mice. After tMCAO, swollen astrocyte end-feet were accompanied by a redistribution of AQP4 in the astrocyte membrane facing not only the basal lamina but also the brain parenchyma. Na$^+$-K$^+$-ATPase β1 is widely expressed in the cytoplasm of various types of cells. Na$^+$-K$^+$-ATPase β1 particles localized in astrocyte end-feet were noticeably reduced in $Ndrg2^{GFAP}$ cKO mice that underwent tMCAO compared to the control mice, and astrocyte end-feet swelling was more serious in the tMCAO groups. We also quantified the protein levels of NDRG2, AQP4 and Na$^+$-K$^+$-ATPase β1 in the ischemic penumbra of the tMCAO mice and the corresponding area of sham-operated mice (Figure 4b,c). AQP4 protein levels increased significantly in $Ndrg2^{GFAP}$ cKO mouse brains compared with control mouse brains in the sham group or tMCAO group. In addition, AQP4 protein levels were upregulated markedly in the MCAO groups compared to the sham groups in both control and $Ndrg2^{GFAP}$ cKO mice. Na$^+$-K$^+$-ATPase β1 protein levels were dramatically reduced in the $Ndrg2^{GFAP}$ cKO brains relative to the control brains in both the sham group and tMCAO group. These data indicate that NDRG2 is necessary for maintaining the polarity and function of astrocytes, which contribute to the structural and functional integrity of the BBB in ischemia.

Interestingly, under physiological conditions, NDRG2 deletion had no significant effect on the astrocyte end-feet area. There may be some reasons explaining this observation. First, NDRG2 was not totally knocked out by the AAV, and the residual NDRG2 in astrocytes still maintained the end-feet area. Second, in vivo experiments may generally involve compensatory molecular signaling pathways and mechanisms that could also maintain the end-feet area of astrocytes. AQP4 and Na$^+$/K$^+$-ATPase are specific molecules that regulate the water balance function of astrocytes. Therefore, we speculated that downregulating NDRG2 expression may directly affect AQP4 and Na$^+$/K$^+$-ATPase expression and some astrocyte functions, such as maintaining water balance, but could not significantly affect the whole end-feet area under physiological conditions.

Using a yeast two-hybrid system and coimmunoprecipitation assay, we previously identified that NDRG2 interacts with Na$^+$-K$^+$-ATPase β1 and regulates the activity of Na$^+$-K$^+$-ATPase β1 in astrocytes (Li, Yang, et al., 2011). To investigate the mechanism underlying the regulation of NDRG2 on ischemic brain edema and the integrity of the BBB, we constructed the AAV pAAV-CAG-MCS-3flag as a control virus and pAAV-CAG-3FLAG-ATP β1 to restore the expression of astrocytic Na$^+$-K$^+$-ATPase β1 in $Ndrg2^{GFAP}$ cKO mice. $Ndrg2^{GFAP}$ cKO
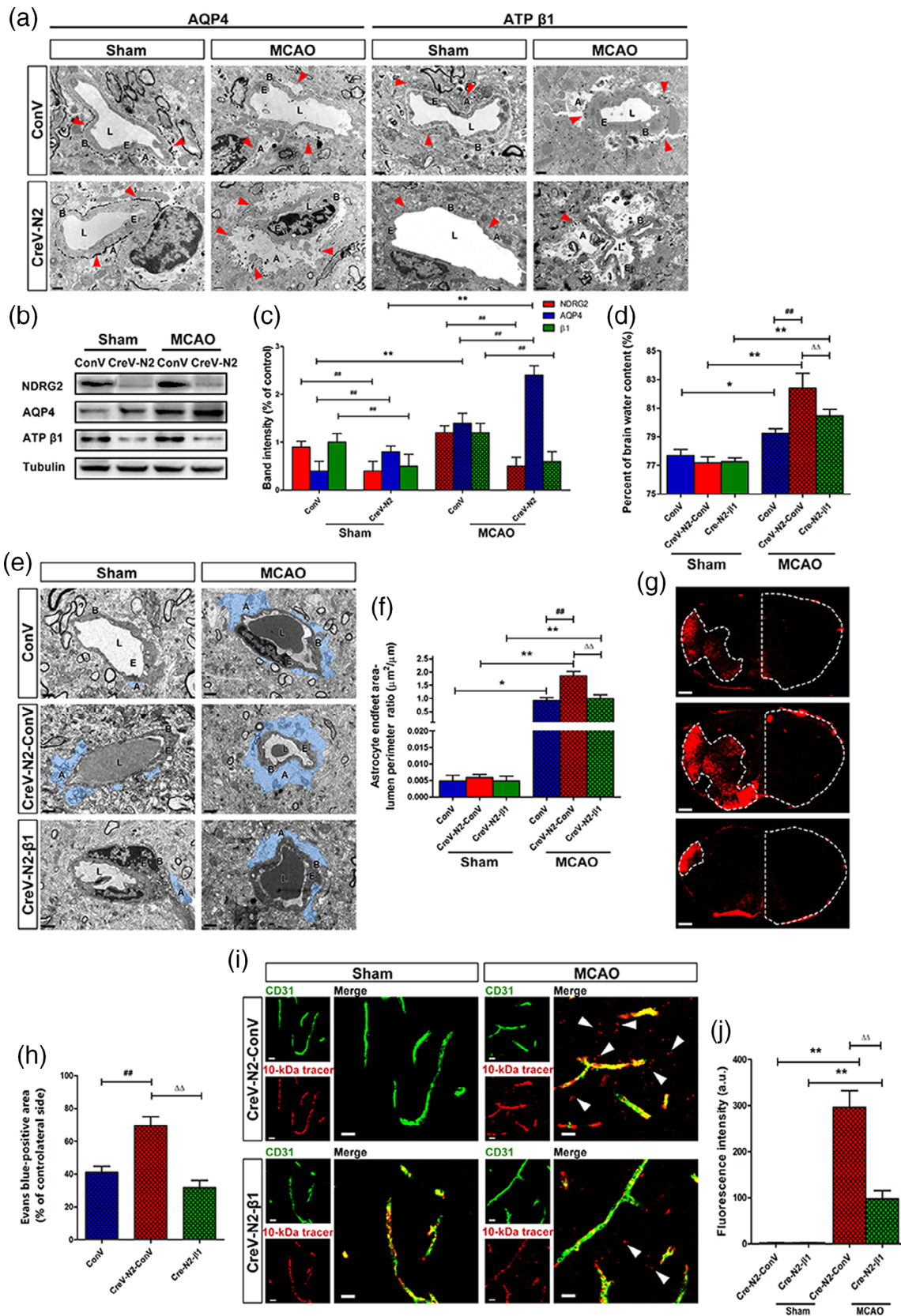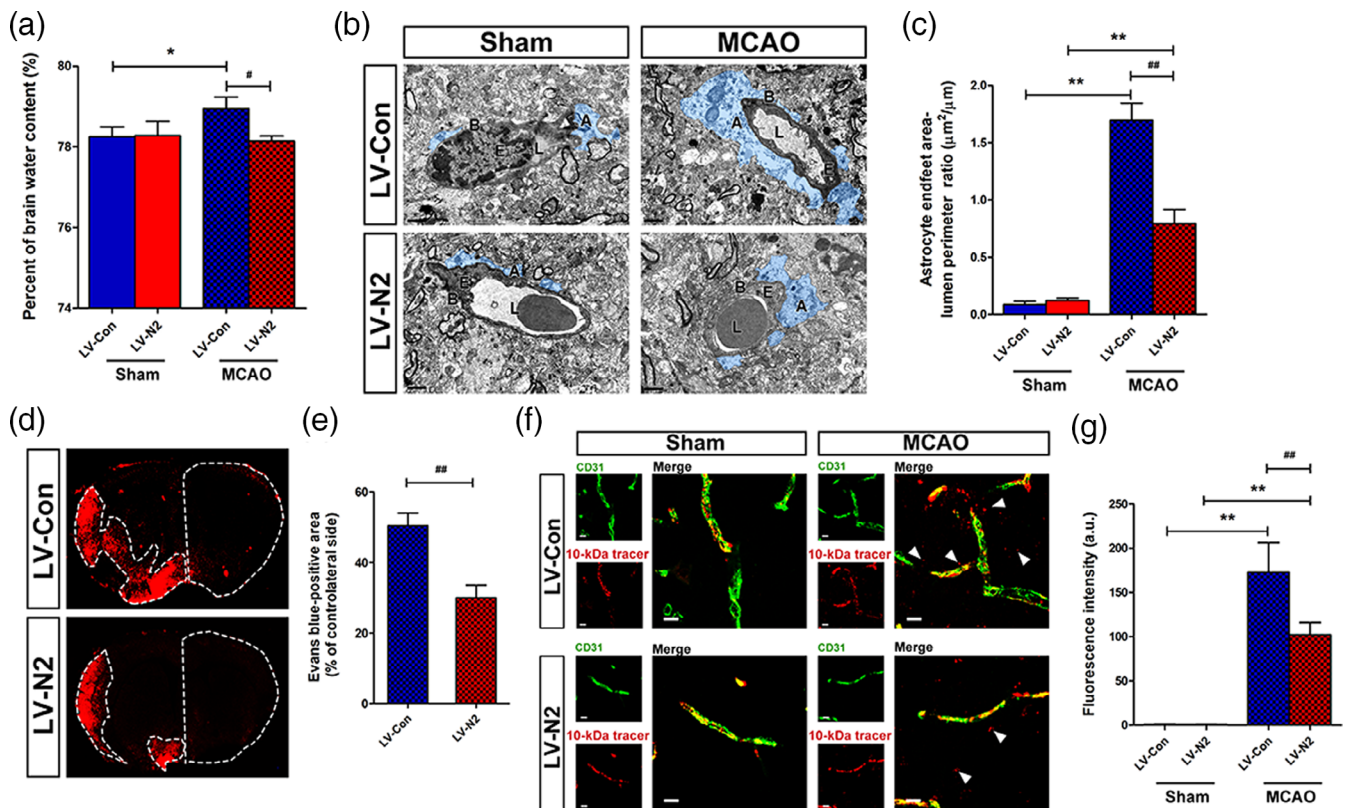
FIGURE 4    Legend on next page.

**FIGURE 5** NDRG2 potential therapeutic effects in ischemic brain edema. (a) Quantification of brain water content in cortices isolated from *Ndrg2*[GFAP] *cKO* mice injected with NDRG2-overexpressing lentivirus (LV-N2) to rescue NDRG2 expression in astrocytes and control virus (LV-Con) in sham groups and MCAO groups. Data are shown as the mean ± *SD* (*n* = 5–6). *$p$ < .05 versus sham mice, #$p$ < .05 versus control mice. (b) Representative transmission electron micrographs showing the swollen perivascular astrocytic end-feet area (blue area) in the NDRG2-rescued group (bottom) and control group (top). A: astrocyte end-feet; B: basal lamina; E: endothelial cell; L: lumen. Scale bar = 2 μm. (c) Astrocyte end-feet area-to-capillary lumen perimeter ratio. Data are shown as the mean ± *SD* (*n* = 5–6). **$p$ < .01 versus sham mice, ##$p$ < .01 versus control mice. (d) Representative images of coronal sections from mice that underwent MCAO after injection of Evans blue dye; fluorescence-positive areas in NDRG2-rescued group (bottom) and control group (top) observed by microscopy. Scale bar = 500 μm. (e) Percent of the area on the contralateral side positive for Evans blue staining. Data are shown as the mean ± *SD* (*n* = 8). ##$p$ < .01 versus control group. (f) The 10-kDa molecular weight tracer was confined to vessels in the sham mice, whereas it leaked out of the vessels (white arrowheads) in the penumbra of the mice that underwent MCAO. Green, CD31; red, tracer. Scale bar = 10 μm. (g) Quantification of tracer fluorescence density (INT/mm$^2$). **$p$ < .01 versus sham group, ##$p$ < .01 versus control group [Color figure can be viewed at wileyonlinelibrary.com]

**FIGURE 4** Na$^+$-K$^+$-ATPase β1 restoration rescues NDRG2 deficiency-mediated BBB disruption and brain edema after stroke. (a) Representative immunoelectron microscopy images of cerebral vessels in the cortices of the sham groups or penumbra zones of the MCAO groups. Red arrowheads indicate subcellular localization of silver-enhanced immunogold labeling of AQP4 or ATP β1 along the BBB. A: astrocyte end-feet; B: basal lamina; E: endothelial cell; L: lumen. Scale bar = 1 μm. (b) Representative Western immunoblots for NDRG2, AQP4, ATP β1, and tubulin using protein extracts from the cortices of the sham groups or penumbra zones of the MCAO groups of *Ndrg2*[GFAP] *cKO* mice or control mice. (c) Densitometric quantification of NDRG2, AQP4 and ATP β1 protein expression is shown normalized to tubulin. Data are expressed as the mean ± *SEM* (*n* = 4). **$p$ < .01 versus sham mice, ##$p$ < .01 versus control mice. (d) Quantification of brain water content in cortices isolated from Na$^+$-K$^+$-ATPase β1-restored *Ndrg2*[GFAP] *cKO* mice (CreV-N2-β1), *Ndrg2*[GFAP] *cKO* mice (CreV-N2-ConV) and control mice (ConV) in the sham and MCAO groups. Data are shown as the mean ± *SD* (*n* = 5–6). *$p$ < .05, **$p$ < .01 versus sham mice, ##$p$ < .01 versus control mice, ΔΔ$p$ < .01 versus *Ndrg2*[GFAP] *cKO* mice. (e) Representative transmission electron micrographs showing the swollen perivascular astrocytic end-feet area (blue area). A: astrocyte end-feet; B: basal lamina; E: endothelial cell; L: lumen. Scale bar = 2 μm. (f) Astrocyte end-feet area-to-capillary lumen perimeter ratio. Data are shown as the mean ± *SD* (*n* = 5–6). *$p$ < .05, **$p$ < .01 versus sham mice, ##$p$ < .01 versus control mice, ΔΔ$p$ < .01 versus *Ndrg2*[GFAP] *cKO* mice. (g) Representative images of coronal sections from mice that underwent MCAO after injection of Evans blue dye; fluorescence-positive areas in Na$^+$-K$^+$-ATPase β1-restored *Ndrg2*[GFAP] *cKO* mice (bottom), *Ndrg2*[GFAP] *cKO* mice (middle), and control mice (top) observed by microscopy. Scale bar = 500 μm. (h) Percentage of the area on the contralateral side positive for Evans blue staining. Data are shown as the mean ± *SD* (*n* = 8). ##$p$ < .01 versus control mice, ΔΔ$p$ < .01 versus *Ndrg2*[GFAP] *cKO* mice. (i) The 10-kDa molecular weight tracer was confined to blood vessels in sham mice, whereas it leaked out of the vessels (white arrowheads) in the penumbra of mice that underwent MCAO. Green, CD31; red, tracer. Scale bar = 10 μm. (j) Quantification of tracer fluorescence density (INT/mm$^2$). **$p$ < .01 versus sham mice, ΔΔ$p$ < .01 versus *Ndrg2*[GFAP] *cKO* mice [Color figure can be viewed at wileyonlinelibrary.com]

mice received right lateral cerebral ventricle injections of pAAV-CAG-MCS-3flag or pAAV-CAG-3FLAG-ATP β1. Three weeks later, the protein levels of NDRG2 and Na$^+$-K$^+$-ATPase β1 in various brain areas (hippocampus, cortex, and striatum) were analyzed (Figure S4a,b). pAAV-CAG-3FLAG-ATP β1 significantly upregulated the protein expression of Na$^+$-K$^+$-ATPase β1 in *Ndrg2*$^{GFAP}$ *cKO* mice. The percentage of brain water content, astrocyte end-feet swelling, and permeation of Evans blue dye and dextran-tetramethylrhodamine (MW, 10 kDa) from the bloodstream into the brain parenchyma were significantly decreased by pAAV-CAG-3FLAG-ATP β1 injection after tMCAO (Figure 4d–j). These data showed that Na$^+$-K$^+$-ATPase rescued the impairment of the BBB under NDRG2 deficiency conditions. Therefore, NDRG2 regulates the polarization and function of astrocytes to maintain the integrity of the BBB by interacting with the Na$^+$-K$^+$-ATPase β1 protein under physiological and pathological conditions.

## 3.5 | NDRG2 protects the brain from ischemic brain edema

To assess the therapeutic potential of NDRG2 on ischemic brain edema, we used a lentivirus that was identified in our previous study to specifically rescue NDRG2 expression in the astrocytes of *Ndrg2*$^{GFAP}$ *cKO* mice (Figure S5). Five days after injection with an NDRG2 overexpression lentivirus in the right lateral cerebral ventricle, the percentage of brain water content was significantly decreased after tMCAO (Figure 5a). TEM showed that the swollen astrocyte end-feet area in the ischemic penumbra of NDRG2-rescued mice was obviously decreased after tMCAO (Figure 5b,c). Barrier permeability was also significantly alleviated in the ischemic penumbra of NDRG2-rescued mouse brains (Figure 5d–g). Taken together, these results imply that NDRG2 has therapeutic potential for ischemic brain edema.

## 4 | DISCUSSION

NDRG2, a well-known tumor suppressor, is mainly expressed in astrocytes in mammalian brains and is upregulated in many neurological disorders, such as ischemia (Li, Shen, et al., 2011), hemorrhage (Gao et al., 2018), trauma (Takarada-Iemata et al., 2014), and Alzheimer's disease (Mitchelmore et al., 2004). Here, we report that NDRG2 deficiency changes the expression and distribution of Na$^+$-K$^+$-ATPase β1 and AQP4, which are involved in the perivascular end-feet of astrocytes in the BBB. NDRG2 deficiency promotes astrocytic swelling and aggravates BBB destruction and brain edema upon ischemic challenge.

Brain edema is a life-threatening consequence of stroke and other cerebral diseases, such as trauma and tumors (Dharmasaroja, 2016; Esquenazi et al., 2017; Jha, Kochanek, & Simard, 2019; Winkler et al., 2016). Current treatments generally include intravascular administration of osmotically active drugs, but such drugs may have only transient effects (Deng et al., 2016; Walcott, Kahle, & Simard, 2012). Thus, novel treatments for brain edema urgently need

to be developed. Brain edema is mainly differentiated into two stages: cytotoxic edema and vasogenic edema. Cytotoxic edema is caused by cerebral vascular occlusion and the subsequent loss of membrane transporter functions, which causes astrocytes to take up more sodium and water from the brain interstitial fluid. Cytotoxic edema is a critical driving force for subsequent processes. Continuous ischemia causes BBB leakage, allowing proteins and cells to intrude into the brain parenchyma from the blood vessels, and vasogenic edema occurs (Simard, Kent, Chen, Tarasov, & Gerzanich, 2007). The two stages of edema could coexist or reciprocally transform, and together, they form the brain edema associated with poor clinical prognosis (Jha et al., 2019; Khanna, Kahle, Walcott, Gerzanich, & Simard, 2014). Previous studies have mainly focused on vasogenic edema, the late stage of ischemic brain edema (Simard et al., 2007). However, interventions targeting this stage did not block the edema source; therefore, these treatments failed in clinical transformation (Cheripelli, Huang, MacIsaac, & Muir, 2016; Sandoval & Witt, 2008). Thus, interventions targeting the cytotoxic swelling stage might provide novel strategies for ischemic brain edema. Astrocyte is one of the major cell types that constitute the BBB (Abbott, Patabendige, Dolman, Yusof, & Begley, 2010; Mathiisen et al., 2010; Zhao, Nelson, Betsholtz, & Zlokovic, 2015). Highly selective channels and transporters, such as AQP4, Na$^+$, K$^+$, and Cl$^-$ transporters, are enriched in the plasma membrane of astrocytes and are implicated in water and ion fluxes (Khanna et al., 2014). The imbalance of astrocytic fluid transport contributes to brain edema; however, the specific molecular mechanism for astrocyte-induced cytotoxic swelling is still not fully understood.

NDRG2 is considered a new marker of mature astrocytes (Flügge et al., 2014; Ma et al., 2014; Okuda, Kokame, & Miyata, 2008; Shen et al., 2008). We previously found that both NDRG2 mRNA and protein expression were increased in mouse brain infarction models (Li, Shen, et al., 2011). Furthermore, we recently found that NDRG2 plays a critical role in facilitating the uptake of glutamate by astrocytes from the interstitial space (Yin et al., 2020), which may protect the brain from glutamate excitotoxicity. NDRG2 was found to maintain the morphology of astrocytes, as *Ndrg2*-silenced astrocytes had shorter processes and lower levels of F-actin than wild-type astrocytes (Takeichi et al., 2011). However, the function of NDRG2 in ischemic brain edema remains to be revealed. Here, we constructed an AAV to conditionally knock out the expression of astroglial NDRG2 and performed transient MCAO in these animals. We found that *Ndrg2* knockout mice exhibited aggravated astrocyte swelling and brain edema after stroke. Astrocytic polarization included both morphological and functional polarization. Maladaptive alterations of astrocytic polarization are the major cause of ischemic brain edema (Gliem et al., 2015; Wang & Parpura, 2016). In the present study, we found that NDRG2 deficiency induced the expression and distribution turbulence of the molecules maintaining astrocytic polarization, such as AQP4 and Na$^+$-K$^+$-ATPase β1.

Na$^+$-K$^+$-ATPase is the primary transporter responsible for Na$^+$, K$^+$, and water transfer in astrocytes (Rose & Karus, 2013). In the cell membrane, Na$^+$-K$^+$-ATPase requires constant energy expenditure to continuously pump out 3 Na$^+$ in exchange for 2 K$^+$ (Kaplan, 2002;

Skou & Esmann, 1992; Sweadner, 1992). This process creates the electric and osmotic neutrality of cells. However, in pathological states, such as brain ischemia, energy depletion leads to Na$^+$-K$^+$-ATPase failure and intracellular Na$^+$ accumulation, generating an osmotic force that drives water influx and cytotoxic cell swelling. The activity of Na$^+$-K$^+$-ATPase reinforced by electroacupuncture maintains ionic balance and relieves cellular edema (Tian, Peng, Cui, Yao, & Li, 2015). Additionally, a recent study showed that Na$^+$-K$^+$-ATPase plays a critical role in the formation and maintenance of intercellular junctions and transdimerization (Tokhtaeva et al., 2012). Our previous study found that NDRG2 binds and stabilizes the β1-subunit of Na$^+$-K$^+$-ATPase to facilitate Na$^+$ transport in human salivary gland epithelial cells (Li, Yang, et al., 2011). In astrocytes, NDRG2 interacts with the β1 subunit of Na$^+$-K$^+$-ATPase and cooperates with this subunit to promote astroglial glutamate uptake (Li et al., 2017). Therefore, NDRG2 and Na$^+$-K$^+$-ATPase are tied to molecular transport. Here, we further identified that NDRG2 is required to maintain the polarization and function of astrocytes by regulating Na$^+$-K$^+$-ATPase β1.

Polarized AQP4 channels are primarily expressed in astrocytic end-feet abutting brain microvessels and contribute to maintaining the polarization of astrocytes and water exchange between brain parenchyma and blood vessels. AQP4 mediates bidirectional water flux, limiting water influx in cytotoxic edema and facilitating water efflux during edema elimination (Saadoun & Papadopoulos, 2010). AQP4 is a passive channel that is modulated by dynamic spatial distribution and the osmotic gradient. AQP4 knockout mice show less brain edema, smaller infarct size and reduced lesion volume after stroke (Hirt et al., 2017). Lower mortality rates and better neurological performance are also observed in these AQP4$^{-/-}$ mice (Hirt et al., 2017; Manley et al., 2000; Yao, Derugin, Manley, & Verkman, 2015). Interestingly, there is a significant increase in the protein levels of AQP4 but no change in mRNA levels in cultured astrocytes exposed to mimic ischemia, suggesting a translational modification of AQP4 upon ischemia (Morishima et al., 2008). In addition, AQP4 expression was found to be changed in a temporal manner (Mogoanta et al., 2014; Stokum et al., 2015; Xiong et al., 2014). In our study, AQP4 expression was dramatically increased and redistributed in a disorderly manner after anoxic and ischemic injury in brain tissues and cultured astrocytes. Therefore, these findings consistently indicated that the change in AQP4 expression is an effect of the pathophysiological conditions underlying edema formation rather than the cause of edema formation.

In conclusion, we identified a protective role of NDRG2 in ischemic brain edema and demonstrated a unique function of NDRG2 in maintaining astrocytic polarization and regulating the integrity of the BBB. We also found that NDRG2 interacts with a key molecule, Na$^+$-K$^+$-ATPase β1, to control brain water content, at least partially. This work indicates that the NDRG2-Na$^+$-K$^+$-ATPase β1 signaling pathway may be a new target for different pathological conditions involving brain edema in the CNS, such as stroke, trauma, tumor, and infectious diseases, and is required for the maintenance of astrocytic polarization.

## CONFLICT OF INTEREST

The authors declare that they have no conflicts of interest.

## DATA AVAILABILITY STATEMENT

Research data are not shared.

## ETHICS STATEMENT

All applicable international and national guidelines for the care and use of animals were followed.

## ORCID

*Yulong Ma* https://orcid.org/0000-0003-0982-9571
*Yan Li* https://orcid.org/0000-0002-7465-7705

## REFERENCES

Abbott, N. J., Patabendige, A. A., Dolman, D. E., Yusof, S. R., & Begley, D. J. (2010). Structure and function of the blood-brain barrier. *Neurobiology of Disease*, 37(1), 13–25. https://doi.org/10.1016/j.nbd.2009.07.030

Alvestad, S., Hammer, J., Hoddevik, E. H., Skare, Ø., Sonnewald, U., Amiry-Moghaddam, M., & Ottersen, O. P. (2013). Mislocalization of AQP4 precedes chronic seizures in the kainate model of temporal lobe epilepsy. *Epilepsy Research*, 105(1–2), 30–41. https://doi.org/10.1016/j.eplepsyres.2013.01.006

Badaut, J., Fukuda, A. M., Jullienne, A., & Petry, K. G. (2014). Aquaporin and brain diseases. *Biochimica et Biophysica Acta*, 1840(5), 1554–1565. https://doi.org/10.1016/j.bbagen.2013.10.032

Cheripelli, B. K., Huang, X., MacIsaac, R., & Muir, K. W. (2016). Interaction of recanalization, intracerebral hemorrhage, and cerebral edema after intravenous thrombolysis. *Stroke*, 47(7), 1761–1767. https://doi.org/10.1161/STROKEAHA.116.013142

Cordonnier, C., Demchuk, A., Ziai, W., & Anderson, C. S. (2018). Intracerebral haemorrhage: Current approaches to acute management. *Lancet*, 392(10154), 1257–1268. https://doi.org/10.1016/S0140-6736(18)31878-6

Deng, Y., Yao, L., Chau, L., Ng, S. S., Peng, Y., Liu, X., et al. (2003). N-Myc downstream-regulated gene 2 (NDRG2) inhibits glioblastoma cell proliferation. *International Journal of Cancer*, 106(3), 342–347. https://doi.org/10.1002/ijc.11228

Deng, Y. Y., Shen, F. C., Xie, D., Han, Q. P., Fang, M., Chen, C. B., & Zeng, H. K. (2016). Progress in drug treatment of cerebral edema. *Mini Reviews in Medicinal Chemistry*, 16(11), 917–925. https://doi.org/10.2174/1389557516666160304151233

Dharmasaroja, P. A. (2016). Fluid intake related to brain edema in acute middle cerebral artery infarction. *Translational Stroke Research*, 7(1), 49–53. https://doi.org/10.1007/s12975-015-0439-1

Dlouhá, H., Teisinger, J., & Vyskocil, F. (1979). Activation of membrane Na+/K+-ATPase of mouse skeletal muscle by acetylcholine and its

inhibition by alpha-bungarotoxin, curare and atropine. *Pflügers Archiv*, *380*(1), 101–104. https://doi.org/10.1007/BF00582620

Eid, T., Lee, T. S., Thomas, M. J., Amiry-Moghaddam, M., Bjørnsen, L. P., Spencer, D. D., … de Lanerolle, N. C. (2005). Loss of perivascular aquaporin 4 may underlie deficient water and K+ homeostasis in the human epileptogenic hippocampus. *Proceedings of the National Academy of Sciences of the United States of America*, *102*(4), 1193–1198. https://doi.org/10.1073/pnas.0409308102

Esquenazi, Y., Lo, V. P., & Lee, K. (2017). Critical care management of cerebral edema in brain tumors. *Journal of Intensive Care Medicine*, *32*(1), 15–24. https://doi.org/10.1177/0885066615619618

Etienne-Manneville, S. (2008). Polarity proteins in glial cell functions. *Current Opinion in Neurobiology*, *18*(5), 488–494. https://doi.org/10.1016/j.conb.2008.09.014

Flügge, G., Araya-Callis, C., Garea-Rodriguez, E., Stadelmann-Nessler, C., & Fuchs, E. (2014). NDRG2 as a marker protein for brain astrocytes. *Cell and Tissue Research*, *357*(1), 31–41. https://doi.org/10.1007/s00441-014-1837-5

Frydenlund, D. S., Bhardwaj, A., Otsuka, T., Mylonakou, M. N., Yasumura, T., Davidson, K. G., … Amiry-Moghaddam, M. (2006). Temporary loss of perivascular aquaporin-4 in neocortex after transient middle cerebral artery occlusion in mice. *Proceedings of the National Academy of Sciences of the United States of America*, *103*(36), 13532–13536. https://doi.org/10.1073/pnas.0605796103

Gao, L., Li, X., Li, H., Li, X., Li, J., Shen, H., & Chen, G. (2018). Spatial-temporal expression of NDRG2 in brain tissues in a rat model of intracerebral hemorrhage: A pilot study. *Neuroscience Letters*, *662*, 356–360. https://doi.org/10.1016/j.neulet.2017.10.021

Gliem, M., Krammes, K., Liaw, L., van Rooijen, N., Hartung, H. P., & Jander, S. (2015). Macrophage-derived osteopontin induces reactive astrocyte polarization and promotes re-establishment of the blood brain barrier after ischemic stroke. *Glia*, *63*(12), 2198–2207. https://doi.org/10.1002/glia.22885

Gorse, K. M., Lantzy, M. K., Lee, E. D., & Lafrenaye, A. D. (2018). Transient receptor potential melastatin 4 induces astrocyte swelling but not death after diffuse traumatic brain injury. *Journal of Neurotrauma*, *35*(14), 1694–1704. https://doi.org/10.1089/neu.2017.5275

Haj-Yasein, N. N., Vindedal, G. F., Eilert-Olsen, M., Gundersen, G. A., Skare, Ø., Laake, P., … Nagelhus, E. A. (2011). Glial-conditional deletion of aquaporin-4 (Aqp4) reduces blood-brain water uptake and confers barrier function on perivascular astrocyte endfeet. *Proceedings of the National Academy of Sciences of the United States of America*, *108*(43), 17815–17820. https://doi.org/10.1073/pnas.1110655108

Hertz, L., Xu, J., Chen, Y., Gibbs, M. E., Du, T., Hertz, L., … Du, T. (2014). Antagonists of the vasopressin V1 receptor and of the beta(1)-adrenoceptor inhibit cytotoxic brain edema in stroke by effects on astrocytes—But the mechanisms differ. *Current Neuropharmacology*, *12*(4), 308–323. https://doi.org/10.2174/1570159X12666140828222723

Hirt, L., Fukuda, A. M., Ambadipudi, K., Rashid, F., Binder, D., Verkman, A., … Badaut, J. (2017). Improved long-term outcome after transient cerebral ischemia in aquaporin-4 knockout mice. *Journal of Cerebral Blood Flow and Metabolism*, *37*(1), 277–290. https://doi.org/10.1177/0271678X15623290

Hwang, J., Kim, Y., Kang, H. B., Jaroszewski, L., Deacon, A. M., Lee, H., et al. (2011). Crystal structure of the human N-Myc downstream-regulated gene 2 protein provides insight into its role as a tumor suppressor. *The Journal of Biological Chemistry*, *286*(14), 12450–12460. https://doi.org/10.1074/jbc.M110.170803

Jayakumar, A. R., Tong, X. Y., Ruiz-Cordero, R., Bregy, A., Bethea, J. R., Bramlett, H. M., & Norenberg, M. D. (2014). Activation of NF-kappaB mediates astrocyte swelling and brain edema in traumatic brain injury. *Journal of Neurotrauma*, *31*(14), 1249–1257. https://doi.org/10.1089/neu.2013.3169

Jha, R. M., Kochanek, P. M., & Simard, J. M. (2019). Pathophysiology and treatment of cerebral edema in traumatic brain injury. *Neuropharmacology*, *145*(Pt B), 230–246. https://doi.org/10.1016/j.neuropharm.2018.08.004

Jukkola, P., & Gu, C. (2015). Regulation of neurovascular coupling in autoimmunity to water and ion channels. *Autoimmunity Reviews*, *14*(3), 258–267. https://doi.org/10.1016/j.autrev.2014.11.010

Kaplan, J. H. (2002). Biochemistry of Na,K-ATPase. *Annual Review of Biochemistry*, *71*, 511–535. https://doi.org/10.1146/annurev.biochem.71.102201.141218

Khanna, A., Kahle, K. T., Walcott, B. P., Gerzanich, V., & Simard, J. M. (2014). Disruption of ion homeostasis in the neurogliovascular unit underlies the pathogenesis of ischemic cerebral edema. *Translational Stroke Research*, *5*(1), 3–16. https://doi.org/10.1007/s12975-013-0307-9

Kimelberg, H. K. (2005). Astrocytic swelling in cerebral ischemia as a possible cause of injury and target for therapy. *Glia*, *50*(4), 389–397. https://doi.org/10.1002/glia.20174

Kitchen, P., Salman, M. M., Halsey, A. M., Clarke-Bland, C., MacDonald, J. A., Ishida, H., … Bill, R. M. (2020). Targeting Aquaporin-4 subcellular localization to treat central nervous system edema. *Cell*, *181*(4), 784–799. https://doi.org/10.1016/j.cell.2020.03.037

Li, Y., Shen, L., Cai, L., Wang, Q., Hou, W., Wang, F., … Xiong, L. (2011). Spatial-temporal expression of NDRG2 in rat brain after focal cerebral ischemia and reperfusion. *Brain Research*, *1382*, 252–258. https://doi.org/10.1016/j.brainres.2011.01.023

Li, Y., Yang, J., Li, S., Zhang, J., Zheng, J., Hou, W., et al. (2011). N-myc downstream-regulated gene 2, a novel estrogen-targeted gene, is involved in the regulation of Na+/K+-ATPase. *The Journal of Biological Chemistry*, *286*(37), 32289–32299. https://doi.org/10.1074/jbc.M111.247825

Li, Y., Yin, A., Sun, X., Zhang, M., Zhang, J., Wang, P., et al. (2017). Deficiency of tumor suppressor NDRG2 leads to attention deficit and hyperactive behavior. *The Journal of Clinical Investigation*, *127*(12), 4270–4284. https://doi.org/10.1172/JCI94455

Lisjak, M., Potokar, M., Rituper, B., Jorgačevski, J., & Zorec, R. (2017). AQP4e-based orthogonal arrays regulate rapid cell volume changes in astrocytes. *The Journal of Neuroscience*, *37*(44), 10748–10756. https://doi.org/10.1523/JNEUROSCI.0776-17.2017

Ma, Y. L., Qin, P., Feng, D. Y., Li, Y., Zhang, L. X., Liu, Z. Y., et al. (2014). Estrogen regulates the expression of Ndrg2 in astrocytes. *Brain Research*, *1569*, 1–8. https://doi.org/10.1016/j.brainres.2014.04.036

Manley, G. T., Fujimura, M., Ma, T., Noshita, N., Filiz, F., Bollen, A. W., … Verkman, A. S. (2000). Aquaporin-4 deletion in mice reduces brain edema after acute water intoxication and ischemic stroke. *Nature Medicine*, *6*(2), 159–163. https://doi.org/10.1038/72256

Mathiisen, T. M., Lehre, K. P., Danbolt, N. C., & Ottersen, O. P. (2010). The perivascular astroglial sheath provides a complete covering of the brain microvessels: An electron microscopic 3D reconstruction. *Glia*, *58*(9), 1094–1103. https://doi.org/10.1002/glia.20990

Menezes, M. J., McClenahan, F. K., Leiton, C. V., Aranmolate, A., Shan, X., & Colognato, H. (2014). The extracellular matrix protein laminin 2 regulates the maturation and function of the blood-brain barrier. *Journal of Neuroscience*, *34*(46), 15260–15280. http://dx.doi.org/10.1523/jneurosci.3678-13.2014.

Minieri, L., Pivonkova, H., Harantova, L., Anderova, M., & Ferroni, S. (2015). Intracellular Na(+) inhibits volume-regulated anion channel in rat cortical astrocytes. *Journal of Neurochemistry*, *132*(3), 286–300. https://doi.org/10.1111/jnc.12962

Mitchelmore, C., Buchmann-Moller, S., Rask, L., West, M. J., Troncoso, J. C., & Jensen, N. A. (2004). NDRG2: A novel Alzheimer's disease associated protein. *Neurobiology of Disease*, *16*(1), 48–58. https://doi.org/10.1016/j.nbd.2004.01.003

Mogoanta, L., Ciurea, M., Pirici, I., Margaritescu, C., Simionescu, C., Ion, D. A., & Pirici, D. (2014). Different dynamics of aquaporin 4 and glutamate transporter-1 distribution in the perineuronal and

perivascular compartments during ischemic stroke. *Brain Pathology*, 24 (5), 475–493. https://doi.org/10.1111/bpa.12134

Morishima, T., Aoyama, M., Iida, Y., Yamamoto, N., Hirate, H., Arima, H., et al. (2008). Lactic acid increases aquaporin 4 expression on the cell membrane of cultured rat astrocytes. *Neuroscience Research*, 61(1), 18–26. https://doi.org/10.1016/j.neures.2008.01.005

Nagelhus, E. A., & Ottersen, O. P. (2013). Physiological roles of aquaporin-4 in brain. *Physiological Reviews*, 93(4), 1543–1562. https://doi.org/10.1152/physrev.00011.2013

Nichols, N. R. (2003). Ndrg2, a novel gene regulated by adrenal steroids and antidepressants, is highly expressed in astrocytes. *Annals of the new York Academy of Sciences*, 1007, 349–356. https://doi.org/10.1196/annals.1286.034

Nico, B., & Ribatti, D. (2012). Morphofunctional aspects of the blood-brain barrier. *Current Drug Metabolism*, 13(1), 50–60. https://doi.org/10.2174/138920012798356970

Okuda, T., Kokame, K., & Miyata, T. (2008). Differential expression patterns of NDRG family proteins in the central nervous system. *The Journal of Histochemistry and Cytochemistry*, 56(2), 175–182. https://doi.org/10.1369/jhc.7A7323.2007

Pillai, A. G., de Jong, D., Kanatsou, S., Krugers, H., Knapman, A., Heinzmann, J. M., … Touma, C. (2012). Dendritic morphology of hippocampal and amygdalar neurons in adolescent mice is resilient to genetic differences in stress reactivity. *PLoS One*, 7(6), e38971. https://doi.org/10.1371/journal.pone.0038971

Quinton, P. M., & Tormey, J. M. (1976). Localization of Na/K-ATPase sites in the secretory and reabsorptive epithelia of perfused eccrine sweat glands: A question to the role of the enzyme in secretion. *The Journal of Membrane Biology*, 29(4), 383–399. https://doi.org/10.1007/BF01868972

Ransom, B. R., & Ransom, C. B. (2012). Astrocytes: Multitalented stars of the central nervous system. *Methods in Molecular Biology*, 814, 3–7. https://doi.org/10.1007/978-1-61779-452-0_1

Relucio, J., Menezes, M. J., Miyagoe-Suzuki, Y., Takeda, S., & Colognato, H. (2012). Laminin regulates postnatal oligodendrocyte production by promoting oligodendrocyte progenitor survival in the subventricular zone. *Glia*, 60(10), 1451–1467. https://doi.org/10.1002/glia.22365

Robinson, J. D. (1975). Mechanisms by which Li+ stimulates the (Na+ and K+)-dependent ATPase. *Biochimica et Biophysica Acta*, 413(3), 459–471. https://doi.org/10.1016/0005-2736(75)90129-7

Rose, C. R., & Karus, C. (2013). Two sides of the same coin: Sodium homeostasis and signaling in astrocytes under physiological and pathophysiological conditions. *Glia*, 61(8), 1191–1205. https://doi.org/10.1002/glia.22492

Rungta, R. L., Choi, H. B., Tyson, J. R., Malik, A., Dissing-Olesen, L., Lin, P. J. C., … MacVicar, B. A. (2015). The cellular mechanisms of neuronal swelling underlying cytotoxic edema. *Cell*, 161(3), 610–621. https://doi.org/10.1016/j.cell.2015.03.029

Saadoun, S., & Papadopoulos, M. C. (2010). Aquaporin-4 in brain and spinal cord oedema. *Neuroscience*, 168(4), 1036–1046. https://doi.org/10.1016/j.neuroscience.2009.08.019

Sandoval, K. E., & Witt, K. A. (2008). Blood-brain barrier tight junction permeability and ischemic stroke. *Neurobiology of Disease*, 32(2), 200–219. https://doi.org/10.1016/j.nbd.2008.08.005

Schindelin, J., Arganda-Carreras, I., Frise, E., Kaynig, V., Longair, M., Pietzsch, T., & Cardona, A. (2012). Fiji: an open-source platform for biological-image analysis. *Nature Methods*, 9(7), 676–682. http://dx.doi.org/10.1038/nmeth.2019.

Shen, L., Zhao, Z. Y., Wang, Y. Z., Ji, S. P., Liu, X. P., Liu, X. W., et al. (2008). Immunohistochemical detection of Ndrg2 in the mouse nervous system. *Neuroreport*, 19(9), 927–931. https://doi.org/10.1097/WNR.0b013e32830163d0

Simard, J. M., Kent, T. A., Chen, M., Tarasov, K. V., & Gerzanich, V. (2007). Brain oedema in focal ischaemia: Molecular pathophysiology and theoretical implications. *Lancet Neurology*, 6(3), 258–268. https://doi.org/10.1016/S1474-4422(07)70055-8

Skou, J. C., & Esmann, M. (1992). The Na,K-ATPase. *Journal of Bioenergetics and Biomembranes*, 24(3), 249–261. https://doi.org/10.1007/BF00768846

Steiner, E., Enzmann, G. U., Lin, S., Ghavampour, S., Hannocks, M. J., Zuber, B., … Engelhardt, B. (2012). Loss of astrocyte polarization upon transient focal brain ischemia as a possible mechanism to counteract early edema formation. *Glia*, 60(11), 1646–1659. https://doi.org/10.1002/glia.22383

Stokum, J. A., Mehta, R. I., Ivanova, S., Yu, E., Gerzanich, V., & Simard, J. M. (2015). Heterogeneity of aquaporin-4 localization and expression after focal cerebral ischemia underlies differences in white versus grey matter swelling. *Acta Neuropathologica Communications*, 3, 61. https://doi.org/10.1186/s40478-015-0239-6

Sweadner, K. J. (1992). Overlapping and diverse distribution of Na-K ATPase isozymes in neurons and glia. *Canadian Journal of Physiology and Pharmacology*, 70(Suppl), S255–S259. https://doi.org/10.1139/y92-269

Takarada-Iemata, M., Kezuka, D., Takeichi, T., Ikawa, M., Hattori, T., Kitao, Y., & Hori, O. (2014). Deletion of N-myc downstream-regulated gene 2 attenuates reactive astrogliosis and inflammatory response in a mouse model of cortical stab injury. *Journal of Neurochemistry*, 130(3), 374–387. https://doi.org/10.1111/jnc.12729

Takarada-Iemata, M., Yoshikawa, A., Ta, H. M., Okitani, N., Nishiuchi, T., Aida, Y., et al. (2018). N-myc downstream-regulated gene 2 protects blood-brain barrier integrity following cerebral ischemia. *Glia*, 66(7), 1432–1446. https://doi.org/10.1002/glia.23315

Takeichi, T., Takarada-Iemata, M., Hashida, K., Sudo, H., Okuda, T., Kokame, K., et al. (2011). The effect of Ndrg2 expression on astroglial activation. *Neurochemistry International*, 59(7), 21–27. https://doi.org/10.1016/j.neuint.2011.03.019

Thrane, A. S., Rangroo Thrane, V., & Nedergaard, M. (2014). Drowning stars: Reassessing the role of astrocytes in brain edema. *Trends in Neurosciences*, 37(11), 620–628. https://doi.org/10.1016/j.tins.2014.08.010

Tian, W. Q., Peng, Y. G., Cui, S. Y., Yao, F. Z., & Li, B. G. (2015). Effects of electroacupuncture of different intensities on energy metabolism of mitochondria of brain cells in rats with cerebral ischemia-reperfusion injury. *Chinese Journal of Integrative Medicine*, 21(8), 618–623. https://doi.org/10.1007/s11655-013-1512-9

Tokhtaeva, E., Sachs, G., Sun, H., Dada, L. A., Sznajder, J. I., & Vagin, O. (2012). Identification of the amino acid region involved in the intercellular interaction between the beta1 subunits of Na+/K+-ATPase. *Journal of Cell Science*, 125(Pt 6), 1605–1616. https://doi.org/10.1242/jcs.100149

Walcott, B. P., Kahle, K. T., & Simard, J. M. (2012). Novel treatment targets for cerebral edema. *Neurotherapeutics*, 9(1), 65–72. https://doi.org/10.1007/s13311-011-0087-4

Wang, Y. F., & Parpura, V. (2016). Central role of maladapted astrocytic plasticity in ischemic brain edema formation. *Frontiers in Cellular Neuroscience*, 10, 129. https://doi.org/10.3389/fncel.2016.00129

Wijdicks, E. F., Sheth, K. N., Carter, B. S., Greer, D. M., Kasner, S. E., Kimberly, W. T., et al. (2014). Recommendations for the management of cerebral and cerebellar infarction with swelling: A statement for healthcare professionals from the American Heart Association/American Stroke Association. *Stroke*, 45(4), 1222–1238. https://doi.org/10.1161/01.str.0000441965.15164.d6

Winkler, E. A., Minter, D., Yue, J. K., & Manley, G. T. (2016). Cerebral edema in traumatic brain injury: Pathophysiology and prospective therapeutic targets. *Neurosurgery Clinics of North America*, 27(4), 473–488. https://doi.org/10.1016/j.nec.2016.05.008

Wolburg, H., Noell, S., Wolburg-Buchholz, K., Mack, A., & Fallier-Becker, P. (2009). Agrin, aquaporin-4, and astrocyte polarity as an important feature of the blood-brain barrier. *The Neuroscientist*, 15(2), 180–193. https://doi.org/10.1177/1073858408329509

Xiong, X. X., Gu, L. J., Shen, J., Kang, X. H., Zheng, Y. Y., Yue, S. B., & Zhu, S. M. (2014). Probenecid protects against transient focal cerebral ischemic injury by inhibiting HMGB1 release and attenuating AQP4 expression in mice. *Neurochemical Research*, *39*(1), 216–224. https://doi.org/10.1007/s11064-013-1212-z

Yang, J., Lunde, L. K., Nuntagij, P., Oguchi, T., Camassa, L. M., Nilsson, L. N., ... Torp, R. (2011). Loss of astrocyte polarization in the tg-ArcSwe mouse model of Alzheimer's disease. *Journal of Alzheimer's Disease*, *27*(4), 711–722. https://doi.org/10.3233/JAD-2011-110725

Yao, L., Zhang, J., & Liu, X. (2008). NDRG2: A Myc-repressed gene involved in cancer and cell stress. *Acta Biochim Biophys Sin*, *40*(7), 625–635. https://doi.org/10.1111/j.1745-7270.2008.00434.x

Yao, X., Derugin, N., Manley, G. T., & Verkman, A. S. (2015). Reduced brain edema and infarct volume in aquaporin-4 deficient mice after transient focal cerebral ischemia. *Neuroscience Letters*, *584*, 368–372. https://doi.org/10.1016/j.neulet.2014.10.040

Yin, A., Guo, H., Tao, L., Cai, G., Wang, Y., Yao, L., ... Li, Y. (2020). NDRG2 protects the brain from excitotoxicity by facilitating interstitial glutamate uptake. *Translational Stroke Research*, *11*(2), 214–227. https://doi.org/10.1007/s12975-019-00708-9

Zhao, Z., Nelson, A. R., Betsholtz, C., & Zlokovic, B. V. (2015). Establishment and dysfunction of the blood-brain barrier. *Cell*, *163*(5), 1064–1078. https://doi.org/10.1016/j.cell.2015.10.067

## SUPPORTING INFORMATION

Additional supporting information may be found online in the Supporting Information section at the end of this article.

**How to cite this article:** H Guo, A Yin, Y Ma, et al. Astroglial N-myc downstream-regulated gene 2 protects the brain from cerebral edema induced by stroke. *Glia*. 2021;69:281–295. https://doi.org/10.1002/glia.23888